Additional hindrance of unfavored α decay between states of different parity

W. M. Seif[1,*] and A. Adel[1,2,†]

[1]*Cairo University, Faculty of Science, Department of Physics, 12613 Giza, Egypt*

[2]*Department of Physics, College of Science in Zulfi, Majmaah University, Majmaah 11952, Saudi Arabia*

(Received 11 January 2019; revised manuscript received 13 March 2019; published 22 April 2019)

We study the influence of the parity configuration of the parent and daughter nuclei on the α-decay process. We consider the ground-state to ground-state favored and unfavored decays, as well as the decay modes to different excited states of the daughter nucleus. The experimental half-life and the calculated decay width based on the realistic M3Y-Paris and the Skyrme-SLy4 effective nucleon-nucleon interactions, within the Wentzel-Kramers-Brillouin approximation, are used to estimate the α-preformation factor for each decay mode. The experimental partial half-lives and α-decay intensities indicate a somewhat larger hindrance of the unfavored decay modes between states of different parities than that of the unfavored decays between states of different spin but with the same parity. This hindrance overcomes the enhancement from a likely increase in the Q_α value of the odd-A isotopes relative to the even-even ones, leading to an increase (decrease) in the half-life (decay intensity) of the decay modes involving a change in parity. We also find that if the states among which the unfavored decay occurs have different parities, the preformation factor of the α cluster inside the parent nucleus becomes less than it would be if the involved states are of the same parity.

DOI: 10.1103/PhysRevC.99.044311

I. INTRODUCTION

α decay is a major decay channel of unstable translead, transuranium, and superheavy nuclei [1–10]. The theoretical investigation of α decay enrich our clear understanding of the correlation between the experimental observables and the different nuclear structure properties, such as the proton and neutron density distribution and the related radii and skin thickness [11–15], nuclear deformation and incompressibility [16,17], the shell and pairing effects [4,9,10], and the impact of the isospin asymmetry [18,19]. Also, it may be appropriately used to get information concerning the ground-state (GS) spin and parity of the involved nuclei [20–23], the nuclear symmetry energy and its density slope [24,25], as well as the half-lives against the other decay modes [26,27]. The α decay mostly leads to a daughter nucleus in its GS. The emitted α particle loads as much energy as possible and the minimal allowed angular momentum. The GS to GS α decay is one possible mode among different decay modes to other states of the daughter nucleus. Each one of these modes has its own branching ratio and partial half-life. The sum of branching ratios (intensities) to the different accessible excited states of the daughter nucleus gives the total α-decay intensity from a certain state of the parent nucleus. The α-decay fine structure offers a valuable tool for determining the spin-parity assignments of the low-lying states [28]. Recently, extensive theoretical studies have been performed on a lot of available high precision data of the α-decay fine structure to investigate the participating transitions and the involved states of the parent and daughter nuclei [8,29–38].

In particular, α decay is very sensitive to the changes of spin-parity configurations between initial and final states [39]. The conservation of angular momentum and parity through α-decay process constrains the possible α transitions to the states of the daughter nucleus that can be populated, and their intensities. α transitions could be classified into two categories: favored and unfavored transitions [39]. For even-even nuclei, α decay preferentially feeds the daughter states that have the same spin and parity as those of the emitting state. Such transitions belong to favored ones which connect states with equal spin and parity [33,40,41]. In such cases, the orbital angular momentum carried by the α particle vanishes, $\ell = 0$. On the contrary, the unfavored transitions occur if the emitting states have different spin and parity assignments from those of the daughter states. In such transitions, α particle carries nonzero orbital angular momentum, $\ell \neq 0$ [30–32,38]. For odd-A and odd(Z)-odd(N) nuclei, the unpaired nucleons could lead to daughter states that differ in spin and parity assignments from those of emitting states yielding to a pronounced hindrance of the additional centrifugal barrier [8,30,31]. Apart from GS to GS transitions, the population of the excited daughter states could be more probable for odd-A and odd-odd nuclei compared to even-even nuclei owing to the unpaired nucleons [30–32]. The investigations of hindered and unhindered α decays enrich our existing knowledge to identify the low-lying states in the daughter nuclei which enable us to obtain further and more detailed information about the excitation energy, decay pattern, possible configurations, and identification of shape staggering [42]. Two kinds of hindrance factors are encountered through the α-decay process. The first one is

*wseif@sci.cu.edu.eg

†ahmedadel@sci.cu.edu.eg

the angular momentum hindrance which originates from the transfer of the nonzero orbital angular momentum. The second one is attributed to a possible structure hindrance that may arise to the nuclear spin orientation and the rearrangement of single-particle orbits [43]. The interplay between these two factors may govern the decay process. This motivates us to investigate both the favored and unfavored decays to the ground state as well as to the different excited states of the daughter nucleus to explore various nuclear structure properties and related quantities.

One of the substantial quantities in describing the α-decay process is the α-particle preformation probability, or the so-called preformation factor S_α. This probability of formation is pivotal to understand how the clusterization of an α particle occurs inside the parent nucleus before its emission through the Coulomb barrier (and centrifugal barrier if angular momentum is transferred) [44–47]. The α-particle preformation probability gains its significance from its correlation with nuclear structure. The α-particle preformation probability was correlated to the neutron and proton level sequences of the parent nucleus [23], which can be used to predict the unknown ground and excited states spins and parities for both even-even and even-odd nuclei [22] as well as odd-even and odd-odd nuclei [20]. Several factors of relevance could influence the α-particle preformation probability, including all the above-mentioned nuclear structure properties [4,9,16,19,48]. Many theoretical attempts have been carried out in recent years to estimate the value of the α-particle preformation probability [4,46–50]. It is worthy of mention that this probability is model dependent but the varying trend of the preformation factor, such as through the isotopic and isotonic chains, is strikingly model independent [51].

The parity is one of the dominant symmetries controlling the quantum transitions. It serves as a common factor in determining the selection rules of nuclear decays and reactions. For instance, it takes part with spin to specify the type of β and α decays. It is recently shown that the different parities of the single proton and neutron in the allowed transition suppress the nuclear matrix elements of β decay [52]. Therefore, we found that it is interesting to investigate to what extent the half-lives and the α-decay intensity are affected for nuclei that unfavorably decay to daughter states of different parity compared to the states of different spin but with the same parity. We also address the question: How will the changes in parity in the two situations affect the α-particle preformation probability? In this regard, all transitions which have experimentally observed α-decay fine structure [53] have been included for the nuclei under study in the present work.

The outline of the paper is as follows. In Sec. II we present the theoretical expressions needed to calculate the interaction potentials between the α and daughter nuclei based on the realistic M3Y-Paris and the Skyrme-SLy4 effective nucleon-nucleon interactions as well as the theoretical formulas used in computing the decay width and extracting the preformation probability. In Sec. III, the available data on the α-decay half-lives and intensities for the considered nuclei, and the calculated results are discussed. Finally, Sec. IV gives a brief conclusion.

II. THEORETICAL FRAMEWORK

In the α-decay fine structure, α transitions could proceed to the GS of the daughter nucleus as well as to the various accessible excited daughter states. If the daughter nucleus is in the excited state i then the Q value must be decreased from the Q value of the GS to GS transition, ($Q_{\mathrm{GS}\to\mathrm{GS}}$), by the excitation energy, E_i^*, as [33,38]

$$Q_i = Q_{\mathrm{GS}\to\mathrm{GS}} - E_i^*. \tag{1}$$

During α-decay process, the allowed values of the orbital angular momentum carried by the α particle are restricted according to the following spin-parity selection rule,

$$|J - J_i| \leqslant \ell \leqslant |J + J_i| \quad \text{and} \quad \frac{\pi_i}{\pi} = (-1)^\ell, \tag{2}$$

where J and J_i are the spins of the parent nucleus and the daughter nucleus in its state i, respectively, while π and π_i are their respective parities. Our calculations have been performed using the minimum possible value of the angular momentum $\ell_{\min}$.

Within the preformed cluster model, the α particle is assumed to exist on the surface of the parent nucleus with a definite preformation probability, before its emission. The preformation factor S_α could be estimated from the experimental α-decay partial half-life time $T_\alpha^{\exp}$, and the calculated partial decay width $\Gamma(Q_i, \ell)$ as

$$S_\alpha = \frac{\hbar \ln 2}{\Gamma(Q_i, \ell)\, T_\alpha^{\exp}}. \tag{3}$$

The calculated partial α-decay width $\Gamma(Q_i, \ell)$ is related to the barrier penetration probability (P_α) and the assault frequency (ν) as $\Gamma(Q_i, \ell) = \hbar\, \nu\, P_\alpha$. The barrier penetration probability P_α can be determined within the well-known Wentzel-Kramers-Brillouin (WKB) approximation by [33,38]

$$P_\alpha = \exp\left(-2 \int_{R_2}^{R_3} \mathrm{d}r \sqrt{\frac{2\,\mu}{\hbar^2} |V_T(r) - Q_i|}\right). \tag{4}$$

Here μ is the reduced mass. R_i ($i = 1, 2, 3$) are the three turning points for the α-daughter potential barrier where $V_T(r)|_{r=R_i} = Q_i$.

The assault frequency of the α particle, ν, can be expressed as [54]

$$\nu = T^{-1} = \frac{\hbar}{2\,\mu}\left[\int_{R_1}^{R_2} \frac{dr}{\sqrt{\frac{2\mu}{\hbar^2} |V_T(r) - Q_i|}}\right]^{-1}. \tag{5}$$

The α-daughter interaction potential is a key factor in the reliable calculations of the α-decay width. In our calculations, the interaction potential is computed microscopically by two methods, namely the double-folding model based on the realistic M3Y-Paris NN interaction [55] with a finite-range exchange part, and the Skyrme energy density formalism using the Skyrme-SLy4 effective NN interaction [56].

The total interaction potential of the α-core system consists of the nuclear, the Coulomb, and the centrifugal

potentials [57],

$$V_{\rm T}(R) = \lambda\, V_N(R) + V_C(R) + \frac{\hbar^2}{2\,\mu}\frac{\left(\ell+\frac{1}{2}\right)^2}{R^2}, \tag{6}$$

where λ is the renormalization factor introduced to the nuclear potential, V_N. R represents the distance between the centers of mass of the α particle and the core. The last term in Eq. (6) represents the centrifugal potential with the Langer modification [54,58]. The value of the renormalization factor λ is computed by applying the Bohr-Sommerfeld quantization condition [54,57],

$$\int_{R_1}^{R_2} dr \sqrt{\frac{2\,\mu}{\hbar^2}\,|V_T(r) - Q_i|} = (G - \ell + 1)\frac{\pi}{2}, \tag{7}$$

where the global quantum number $G = 20\,(N > 126)$ and $G = 18\,(82 < N \leqslant 126)$ [57].

Within the double-folding model [59], the nuclear part of the potential $V_N(R)$ is the sum of two terms, the direct $V_D(R)$ and the exchange $V_{\rm Ex}(R)$ parts, which are given by [60]

$$V_D(R) = \int d\vec{r}_1 \int d\vec{r}_2\; \rho_\alpha(\vec{r}_1)\, \upsilon_D(s)\, \rho_d(\vec{r}_2), \tag{8}$$

$$V_{\rm Ex}(R) = \int d\vec{r}_1 \int d\vec{r}_2\; \rho_\alpha(\vec{r}_1, \vec{r}_1 + \vec{s})\, \rho_d(\vec{r}_2, \vec{r}_2 - \vec{s}) \times \upsilon_{\rm Ex}(s) \exp\left[\frac{i\,\vec{k}(R)\cdot\vec{s}}{M}\right]. \tag{9}$$

Here $\vec{s}$ is the NN separation vector. $\rho_\alpha(\vec{r}_1)$ and $\rho_d(\vec{r}_2)$ are the density distributions of the α particle and the daughter nucleus, respectively, and $M = A_1\,A_2/(A_1 + A_2)$. The relative-motion momentum $k(r)$ is given by $k^2(r) = 2\,\mu\,[E_{\rm c.m.} - V_N(r) - V_C(r)]/\hbar^2$. $E_{\rm c.m.}$ represents the center-of-mass energy.

The Coulomb potential can be calculated within the double-folding model in terms of the proton-proton Coulomb interaction (e^2/s) and the involved proton densities as

$$V_C(r) = \iint \rho_{p\alpha}(\vec{r}_1)\, \upsilon_C(s)\, \rho_{pd}(\vec{r}_2) d\vec{r}_1 d\vec{r}_2. \tag{10}$$

In our calculations we have used a realistic M3Y-Paris effective NN interaction, which has the form [55,59],

$$\upsilon_D(s) = \left[11061.625\,\frac{e^{-4s}}{4\,s} - 2537.5\,\frac{e^{-2.5s}}{2.5\,s}\right], \tag{11}$$

$$\upsilon_{Ex}(s) = \left[-1524.25\,\frac{e^{-4s}}{4\,s} - 518.75\,\frac{e^{-2.5s}}{2.5\,s} - 7.8474\,\frac{e^{-0.7072s}}{0.7072\,s}\right]. \tag{12}$$

The method of calculating the double-folding nuclear and Coulomb potentials can be found in more detail in Refs. [33,60].

On the other hand, the nucleus-nucleus interaction potential $V(R)$ is defined in the framework of the Skyrme energy density formalism [4,61–63] as the difference between the energy E_{12} of the interacting nuclei that are overlapping and that of those completely separated $E_{1(2)}$ at infinity,

$$\begin{aligned} V(R) &= E_{12}(R) - E_1 - E_2 \\ &= \int H[\rho_{p\alpha}(\vec{r}) + \rho_{pD}(\vec{R},\vec{r}),\, \rho_{n\alpha}(\vec{r}) + \rho_{nD}(\vec{R},\vec{r})]d\vec{r} \\ &\quad - \int H[\rho_{p\alpha}(\vec{r}),\, \rho_{n\alpha}(\vec{r})]d\vec{r} - \int H[\rho_{pD}(\vec{r}),\, \rho_{nD}(\vec{r})]d\vec{r}, \end{aligned} \tag{13}$$

where $\rho_{ij}(i = p, n$ and $j = \alpha, D)$ are the frozen density distributions of the protons (p) and neutrons (n) associated to α and daughter (D) nuclei. The energy density functional H is given by [4,25,56,61]

$$H(\rho_i, \tau_i, \vec{J}_i) = \frac{\hbar^2}{2m}\sum_{i=n,p}\tau_i(\rho_i, \vec{\nabla}\rho_i, \nabla^2\rho_i) + H_{\rm Sky}(\rho_i, \tau_i, \vec{J}_i) + H_C(\rho_p), \tag{14}$$

where $\tau_{i=p,n}$ and $\vec{J}_{i=p,n}$ define, respectively, the kinetic energy and the spin-orbit densities. The explicit forms of the nuclear ($H_{\rm Sky}$) and the Coulomb (H_C) energy density functionals, the Skyrme-SLy4 parametrization that is used in the present calculations, and more details about the method of calculations based on the Skyrme-SLy4 NN interaction are given in Refs. [4,25,56,61].

III. RESULTS AND DISCUSSION

The α decays are abundantly observed for the nuclei in the translead and transuranium regions, with half-lives extending from nanoseconds up to millions of years. Figure 1 shows the partial half-lives against α-decay for the ground-state (GS) to ground-state favored and unfavored decay modes of the Pu, Cm, Cf, and Fm isotopes. Sixteen plutonium isotopes ($^{228-242,244}$Pu) are known to be α emitters. The spin-parity assignments of these isotopes and of their daughter isotopes ($^{224-238,240}$U), the α-decay half-life, and the intensity of their GS to GS α-decay modes are fortunately known [53,64]. Nonexperimental $J^\pi = 5/2^+$ was systematically assigned to the ground states of ^{233}Pu and ^{225}U [64]. The GS to GS α decays of the nine even(Z)-even(N) ^{228,230,232,234,236,238,240,242,244}Pu(0^+) isotopes are all favored decay modes between states of the same spin parity. Within the shell model, the orbitals $3d_{3/2}$, $3d_{5/2}$, and $4s_{1/2}$ that have positive parity are among the orbitals available for an odd valence neutron above $N = 126$. This explains the ground-state configurations of the even-odd ^{229,231}Pu($3/2^+$), ^{233,235,241}Pu($5/2^+$), and ^{239}Pu($1/2^+$) isotopes. ^{237}Pu($7/2^-$) is the only Pu α emitter of a GS with a negative parity. In contrast to the favored decay ^{231}Pu($3/2^+$) $\rightarrow$ ^{227}U($3/2^+$), the ^{229}Pu($3/2^+$) $\rightarrow$ ^{225}U($5/2^+$), ^{233}Pu($5/2^+$) $\rightarrow$ ^{229}U($3/2^+$), and ^{241}Pu($5/2^+$) $\rightarrow$ ^{237}U($1/2^+$) decays are unfavored decays between ground states of different spins but with similar parities. However, the decays ^{235}Pu($5/2^+$) $\rightarrow$ ^{231}U($5/2^-$), ^{237}Pu($7/2^-$) $\rightarrow$ ^{233}U($5/2^+$), and ^{239}Pu($1/2^+$) $\rightarrow$ ^{235}U($7/2^-$) are the only α decays of Pu between ground states of different parities. In Fig. 1, the

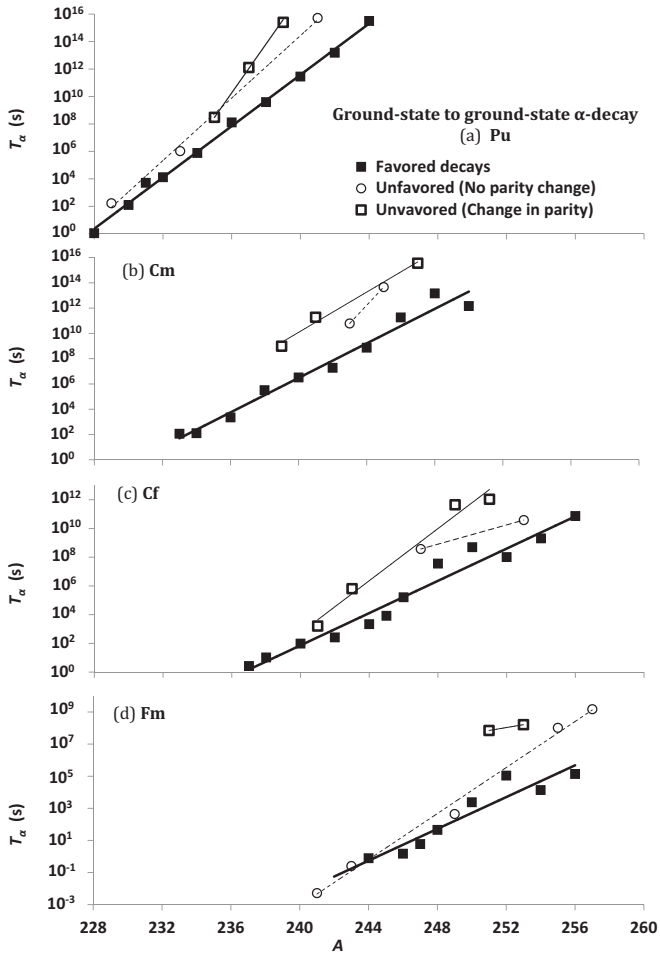

FIG. 1. The observed partial half-lives T_α (s) [53], on a logarithmic scale, for the GS to GS α-decay modes of the (a) $^{228-242,244}$Pu, (b) $^{233,234,236,238-248,250}$Cm, (c) $^{237,238,240-254,256}$Cf, and (d) $^{241,243,244,246-257}$Fm isotopes, as a function of the mass number A. While the favored decay modes between ground states of the same spin parity are shown as solid squares, the unfavored decay modes between ground states of the same (different) parities are shown as open circles (squares). The straight lines show the trendline for the different decay types.

half-lives of the favored decay modes are represented by the solid squares, while the open circles (squares) denote unfavored decays between states of the same (different) parties. Whereas the average branching ratio (intensity) for the 10 favored α-decay modes of Pu is 57.99%, that corresponds to the three unfavored decay modes between ground states of similar (different) parities is 3.37% (0.01%). In particular, the intensities of the GS to GS decay modes of ^{235}Pu$(5/2^+)$, ^{237}Pu$(7/2^-)$, and ^{239}Pu$(1/2^+)$ are about 0.0005%, 0.0003%, and 0.03% [53], respectively. While the total α-decay intensity of ^{239}Pu$(1/2^+)$ is 100%, most of this intensity appears via its decay modes to the $5/2^+$ (11.94%), $1/2^+$ (70.71%), and $3/2^+$ (17.11%) excited states of ^{235}U, which have the same positive parity. Also, most of the total α-decay intensity of ^{235}Pu$(5/2^+, 0.0027\%)$ and ^{237}Pu$(7/2^-, 0.0042\%)$ appears in their decay modes to the excited states of ^{231}U$(5/2^+, 0.0022\%)$ and ^{233}U$(7/2^-, 5/2^-, 9/2^-; 0.0030\%)$, respectively, with no change in parity. Figure 1 shows that the half-lives of the presented isotopes commonly increase with the mass number A. However, the partial half-life of the α-decay mode of ^{235}Pu $(5/2^+, Q_\alpha = 5.951$ MeV, $T_\alpha = 3.04 \times 10^8$ s$) \rightarrow$ ^{231}U$(5/2^-)$ that involves a change in parity is 132% larger than that of the decay mode ^{236}Pu$(0^+, Q_\alpha = 5.867$ MeV, $T_\alpha = 1.31 \times 10^8$ s$)$ $\rightarrow$ ^{232}U(0^+) between states of similar parity, even though the former has larger Q_α. Similarly, the decay mode ^{237}Pu $(7/2^-, Q_\alpha = 5.748$ MeV, $T_\alpha = 1.30 \times 10^{12}$ s$)$ $\rightarrow$ ^{233}U$(5/2^+)$ between states of different parities shows roughly 3 orders of magnitude larger half-life than the next decay mode of ^{238}Pu $(0^+, Q_\alpha = 5.593$ MeV, $T_\alpha = 3.90 \times 10^9$ s$)$ $\rightarrow$ ^{234}U(0^+) between states of similar parity. It is also larger than T_α of the GS to GS decay mode of heavier ^{240}Pu isotope. Likewise, the decay mode of ^{239}Pu $(1/2^+, Q_\alpha = 5.245$ MeV, $T_\alpha = 2.54 \times 10^{15}$ s$)$ $\rightarrow$ ^{235}U$(7/2^-)$, between states of different parities, has 4 and 2 orders of magnitude larger T_α than the decay modes of ^{240}Pu $(0^+, Q_\alpha = 5.256$ MeV, $T_\alpha = 2.84 \times 10^{11}$ s$)$ $\rightarrow$ ^{236}U(0^+) and ^{242}Pu $(0^+, Q_\alpha = 4.985$ MeV, $T_\alpha = 1.54 \times 10^{13}$ s$)$ $\rightarrow$ ^{238}U(0^+), respectively. On the other hand, T_α of the unfavored GS to GS decay mode of ^{229}Pu$(3/2^+)$ is about 30% larger than that of the favored decay of the next ^{230}Pu(0^+) isotope. Also, the GS to GS unfavored decay modes of ^{233,241}Pu$(5/2^+)$ show one and two orders of magnitude larger T_α than the favored decays of their next ^{234,242}Pu(0^+) isotopes. This indicates that the hindrance in the unfavored α-decay modes that involve a change in parity is larger than that of the unfavored decays between states of similar parities.

Fifteen curium ($^{233,234,236,238-248,250}$Cm), 18 californium ($^{237,238,240-254,256}$Cf) and 15 fermium ($^{241,243,244,246-257}$Fm) isotopes are α emitters with known spin-parity assignments of the involved parent and daughter isotopes, intensity, and T_α of their GS to GS α-decay modes [53,64]. Nonexperimental GS spin-parity configurations were systematically assigned to a few participating nuclei, namely ^{237}Cm$(5/2^+)$, ^{239}Cf$(5/2^+)$, ^{241}Fm$(5/2^+)$, and ^{245}Fm$(1/2^+)$ [64]. Among the mentioned GS to GS decays, only the decays of ^{239,241,247}Cm, ^{241,243,249,251}Cf, and ^{251,253}Fm take places between ground states of different parities. In addition to the GS to GS favored decays of their even-even isotopes, the decays of ^{233}Cm$(3/2^+)$, ^{237}Cf$(3/2^+)$, ^{245}Cf$(1/2^+)$, and ^{247}Fm$(1/2^+)$ are also favored decays between even-odd nuclei of similar spin-party assignments. The GS to GS decays of ^{243}Cm$(5/2^+)$, ^{245}Cm$(7/2^+)$, ^{247,253}Cf$(7/2^+)$, ^{241}Fm$(5/2^+)$, ^{243,249,255}Fm$(7/2^+)$, and ^{259}Fm$(9/2^+)$ are unfavored decays between nuclei of different spin, but with the same parity. The average intensity for the 30 favored GS to GS α decays of the Cm, Cf, and Fm isotopes is 50.44%. The nine unfavored decay modes between ground states of the same parity for the three sets of isotopes show an average intensity of 15.89%. The corresponding nine unfavored decay modes between ground states of different parities is 3.68%. For instance, the total intensity of α decay of the ^{249}Cf$(9/2^-)$ isotope to ^{245}Cm in its different states is 100%, which was observed through 31 α-decay modes. Most of this intensity

corresponds to the favored decay mode to the excited state of ^{245}Cm ($9/2^-$ ($E = 0.388$ MeV), $I_\alpha = 82.2\%$) and the unfavored decay to $11/2^-$($E = 0.443$ MeV, 4.69%), which have the same negative parity of ^{249}Cf($9/2^-$). The highest intense decay modes between states of different parities were observed to the excited states $5/2^+$ ($E = 0.253$ MeV, 3.33%) and $7/2^+$ (0.296 MeV, 3.21%), as well as to the GS of ^{245}Cm ($7/2^+$, 2.46%). The total intensity of the decay modes between states of different parities is about 12.43%, whereas that corresponding to decays between states of the same parity is about 87.36%. The detailed intensity distribution of ^{251}Cf($1/2^+$, $I_\alpha \approx 100\%$) and ^{247}Cm($9/2^-$, 100%) will be discussed below.

In contrast with the general increasing trend of T_α with A shown in Fig. 1(b), the GS to GS α-decay modes of ^{239}Cm ($7/2^-$, $Q_\alpha = 6.540$ MeV [65]), ^{241}Cm ($1/2^+$, 6.185 MeV) [66], and ^{247}Cm ($9/2^-$, 5.354 MeV) that involve a change in parity exhibit, respectively, 3, 4, and 2 orders of magnitude larger T_α than the favored decays of their next ^{240}Cm (0^+, 6.397 MeV), ^{242}Cm (0^+, 6.216 MeV), and ^{248}Cm (0^+, 5.162 MeV) isotopes. On the other hand, the corresponding unfavored decay modes of ^{243}Cm ($5/2^+$, 6.169 MeV) and ^{245}Cm ($7/2^+$, 5.625 MeV) that involve no change in parity show less increase of T_α of about 2 orders of magnitude larger than that of favored decays of their next ^{244}Cm (0^+, 5.902 MeV) and ^{246}Cm (0^+, 5.475 MeV) isotopes. Even T_α of the unfavored decay mode of ^{241}Cm ($1/2^+$) that involves a change in parity is 211% larger than that of the next unfavored decay of ^{243}Cm ($5/2^+$) between states of similar parity, although the former has larger Q_α. Moreover, the mentioned decays of ^{239}Cm ($7/2^-$), ^{241}Cm ($1/2^+$), and ^{247}Cm ($9/2^-$) show larger T_α than that of the ^{242,244}Cm (0^+), ^{244,246}Cm (0^+), and ^{250}Cm (0^+) isotopes, respectively. In the same manner, Fig. 1(c) shows that the decay modes of ^{241}Cf ($7/2^-$), ^{243}Cf ($1/2^+$), ^{249}Cf ($9/2^-$), and ^{251}Cf ($1/2^+$) between ground states of different parities have larger T_α than that of the favored decays of ^{242}Cf, ^{244,245,246}Cf, ^{250,252,254,256}Cf, and ^{252,254,256}Cf, respectively. The observed respective increase in T_α reaches 4 orders of magnitude. The increase in the T_α of the unfavored decay modes of ^{247,253}Cf ($7/2^+$) to ^{243}Cm ($5/2^+$) and ^{249}Cm ($1/2^+$), which have the same parity, relative to that of the GS to GS decays of their next ^{248,254}Cf isotopes is only 1 order of magnitude. It is also noteworthy that the decay modes of ^{249}Cf ($9/2^-$, Q_α=6.293 MeV, $T_\alpha = 4.50 \times 10^{11}$ s) $\rightarrow$ ^{245}Cm($7/2^+$), and ^{251}Cf ($1/2^+$, 6.177 MeV, 1.09×10^{12} s)$\rightarrow$ ^{247}Cm($9/2^-$) between ground states of different parities exhibit 1 and 2 orders of magnitude larger half-lives than the unfavored decay of ^{253}Cf ($7/2^+$, 6.126 MeV, 3.85×10^{10} s) to ^{249}Cm ($1/2^+$), which have the same parity. Similar behavior can be seen in Fig. 1(d) for the Fm isotopes where the decay modes of ^{251}Fm ($9/2^-$) and ^{253}Fm ($1/2^+$) that involve a change in parity show longer partial half-lives than those of the favored decays of their next ^{252,254,256}Fm (0^+) and ^{254,256}Fm(0^+) isotopes, respectively. This increase of T_α amounts to about 4 orders of magnitude. T_α of the unfavored decay mode of ^{255}Fm($7/2^+$) to ^{251}Cf ($1/2^+$) that has a similar parity is 3 orders of magnitude larger than that of the favored decay of its next ^{256}Fm(0^+) isotope. The decay mode of ^{253}Fm($1/2^+$) $\rightarrow$ ^{249}Cf($9/2^-$) between ground states of different parities is itself 57% larger than the unfavored decay of ^{255}Fm($7/2^+$) $\rightarrow$ ^{251}Cf($1/2^+$). A common feature that can be seen in the different panels of Fig. 1 is that the increasing trendline of the unfavored decays between ground states of the same parity tends to lie below that corresponding to the unfavored decays between states of different parity, in which both lie above the trendline of the favored decays. The data presented in Fig. 1 and the details discussed above reflect a somewhat stronger hindrance of the α decays involving a change in parity than that already reported for the unfavored decays in general, with respect to the favored decays. This hindrance can overcome the expected decrease in half-life from a likely increase in Q_α of the odd-A isotopes with respect to the even-even ones.

To investigate the decay modes to excited states, presented in Figs. 2(a) and 2(b) are the extracted α-preformation factor S_α for the α-decay processes of the even-even ^{226,228,230}Th isotopes in their ground state (0^+) into the ground and different excited states of their ^{222,224,226}Ra daughter nuclei. For a particular decay mode to a given state (J^π_D) of the daughter nucleus, the preformation factor is extracted from the corresponding experimental partial half-life and the calculated decay width, $S_\alpha(J^\pi_{P,D}) = \hbar \ln 2/\Gamma(J^\pi_{P,D})T^{\rm exp}_\alpha(J^\pi_{P,D})$, Eq. (3). For such calculations in which the wave states of the involved nuclei are not explicitly taken into account, structural effects are contained in the used Q_α value, in the considered transferred angular momentum, and in the in the extracted α-preformation factor. S_α is plotted in Figs. 2(a) and 2(b) as a function of the quantum number $\ell_{\rm min}$ corresponding to the minimum allowed angular momentum transferred by the emitted α particle. The calculated decay widths based on the M3Y-Paris and the Skyrme-SLy4 *NN* interactions are used to deduce S_α in Figs. 2(a) and 2(b), respectively. In Fig. 2, the results for the decay modes that demand a change in parity (open symbols) are compared to those involving no change in parity (solid symbols), for the same parent and daughter isotopes. The solid line connects the average values for the same $\ell_{\rm min}$. The three ^{226,228,230}Th isotopes decay via α decay with an intensity of 100%. They mainly decay to the ground state (0^+) of their daughter nuclei with an intensity of 75.5%, 73.4%, and 76.3% [53], respectively. The next intense decay modes take places to the ^{222,224,226}Ra isotopes in their 2^+ state with branching ratios of 22.8%, 26%, and 23.4%, respectively. These decay modes involve no change in parity. The decay modes involving a change in parity appear as the third intense decay mode to ^{222,224}Ra(1^-) and the fourth decay mode to ^{226}Ra(1^-), at low branching ratios of 1.26%, 0.408%, and 0.03%, respectively. The decay modes between states of different parities represent only 1.47%, 0.44%, and 0.03% of the full α-decay intensity of ^{226,228,230}Th(0^+), respectively. As an example, the intensity of nine decay modes of ^{228}Th(0^+) to different states of ^{224}Ra (0^+($E = 0$ MeV), 2^+ (0.084 MeV), 1^-, 4^+, 3^-, 5^-, 6^+, 0^+ (0.916 MeV), 2^+ (0.993 MeV) are shown in Fig. 2(c), as a function of $\ell_{\rm min}$. Figure 2(c) and the intensities of the decay modes to the ground and excited states of ^{222,226}Ra confirm that the α-decay intensity relatively decreases for the decay modes involving a change in parity.

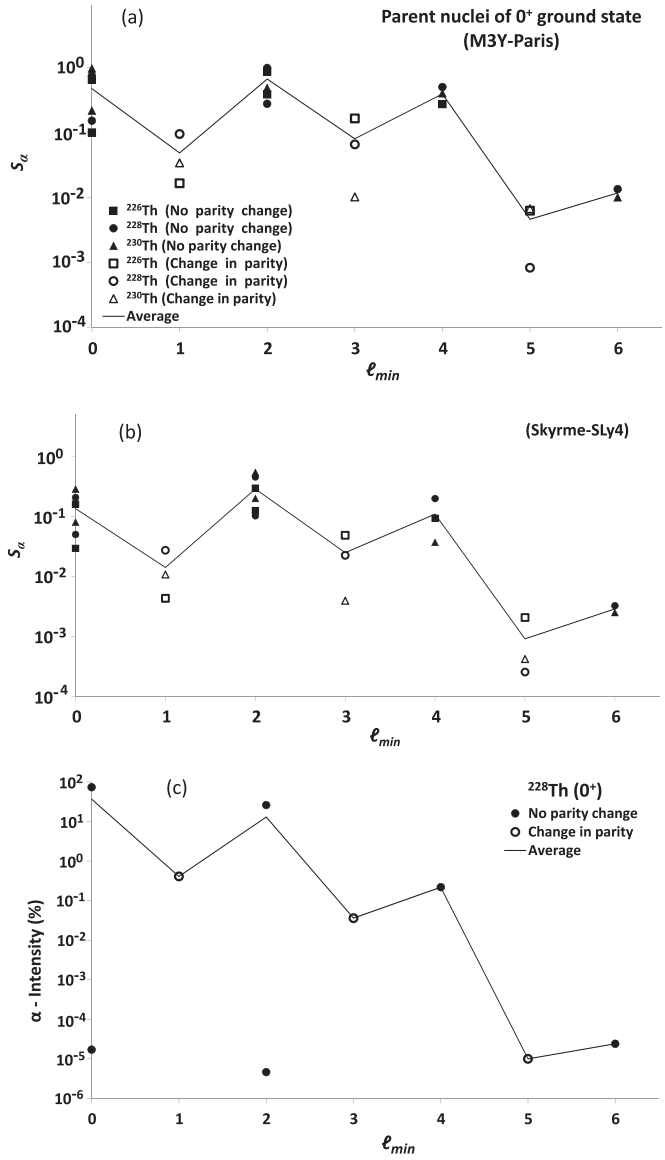

FIG. 2. The α preformation factor S_α ($T_\alpha^{\rm exp}$, $\Gamma_\alpha^{\rm cal}$), on a logarithmic scale, for the α-decay modes of the even-even ^{226,228,230}Th(0^+) isotopes to the different states of the ^{222,224,226}Ra daughter isotopes, as extracted from the experimental partial half-life $T_\alpha^{\rm exp}$ and the calculated decay width $\Gamma_\alpha^{\rm cal}$ based on (a) M3Y-Paris and (b) Skyrme-SLy4 NN interactions. S_α is plotted versus the quantum number $\ell_{\rm min}$ defining the minimum angular momentum transferred by the α particle. While the solid symbols represent the unfavored decays between states of the same parity (even $\ell_{\rm min}$), the open ones represent unfavored decays between states of different parities (odd $\ell_{\rm min}$). (c) The intensity I_α of the α-decay modes of ^{228}Th(0^+) to the different states of ^{224}Ra, as a function of $\ell_{\rm min}$. The solid curves show the average values of S_α ($\ell_{\rm min}$) and I_α ($\ell_{\rm min}$).

The decrease in the intensity of the decay modes to the higher 0^+ (0.916 MeV) and 2^+ (0.993 MeV) excited states of ^{224}Ra with respect to that of the lower 0^+ (0 MeV) and 2^+ (0.084 MeV) states is understood as a consequence of decreasing the corresponding Q values. Generally, Fig. 2(a) shows an oscillatory behavior for S_α and its average values $S_\alpha^{\rm ave}$ as functions of $\ell_{\rm min}$, with several local maxima and minima. The local maxima of $S_\alpha^{\rm ave}(\ell_{\rm min})$ are all obtained at the even values of $\ell_{\rm min}$, which correspond to decay modes with no parity change. Each local maximum is followed by a local minimum at the next odd $\ell_{\rm min}$ value. Of course, the odd values of $\ell_{\rm min}$ identify the decay modes with a parity change. The extracted preformation factors from the decay widths based on the Skyrme-SLy4 *NN* interaction in Fig. 2(b) typically confirm the obtained behavior of $S_\alpha(\ell_{\rm min})$ in Fig. 2(a). The decrease in the preformation factors for the decay modes with a change in parity emphasizes the hindrance of such decays from the involved parity change. The ratios of the preformation factors of the ^{226,228,230}Th unfavored decay modes to that of their favored decays are presented in Table I. Such ratios effectively display the structure effects. Table I shows that the unfavored decay modes that involve a change in parity exhibit less relative S_α values, with respect to that of the corresponding favored decays, than the decays taking places between states of the same parity. While the S_α(unfavored)/S_α(favored) ratios for the ^{226,228,230}Th decay modes between states of the same parity range between 0.010 and 1.343 (with an average value of 0.608), they range between 0.001 and 0.254 (with an average of 0.062) for the decay modes between states of different parities.

In Fig. 3(a), the estimated α-preformation factor is displayed versus $\ell_{\rm min}$ for the decay modes of the even(Z)-odd(N) ^{225}Th($3/2^+$), ^{251}Cf($1/2^+$), and ^{255}Fm($7/2^+$) nuclei in their ground states into the ground states of their ^{221}Ra($5/2^+$), ^{247}Cm($9/2^-$), and ^{251}Cf($1/2^+$) daughters, and into their different excited states as well. The experimental partial half-lives and the calculated decay widths based on the M3Y-Paris interaction are used to extract S_α in Fig. 3(a). The ^{225}Th, ^{251}Cf, and ^{255}Fm nuclei in their non-zero-spin and positive parity ground states mainly decay through α decay with intensities of 90%, 100%, and 100%, respectively, in addition to minor electron capture (^{225}Th) and spontaneous fission (^{251}Cf and ^{255}Fm) modes. The α decays involving a change in parities contribute to only 8.10%, 15.70%, and 0.05% of the mentioned α-decay intensities of ^{225}Th($3/2^+$), ^{251}Cf($1/2^+$), and ^{255}Fm($7/2^+$), respectively. For ^{225}Th($3/2^+$), the three highest intense decay modes were observed to the three excited states $3/2^+$ (E = 0.321 MeV, $I_\alpha = 39\%$, $\ell_{\rm min} = 0$), $5/2^+$ (0.359 MeV, 13.5%, 2), and $7/2^+$ (0.299 MeV, 12.6%, 2) of ^{221}Ra. The decay to the ground state of ^{221}Ra ($5/2^+$(0 MeV, 8.1%, 2) appeared as the fourth intense decay mode. The appearance of the decay mode to the state $3/2^+$ (0.321 MeV, 39%, 0) of ^{221}Ra as the highest intense mode is understood where the decay modes between two states of the same spin-parity configuration is favored. The sixth intense decay mode to the state $7/2^-$ (0.147 MeV, 2.7%, 3) of ^{221}Ra was observed as the first decay mode with a change in parity, even it has lower energy than the mentioned first three states ($3/2^+$, $5/2^+$, and $7/2^+$) of ^{221}Ra. For ^{251}Cf($1/2^+$) and ^{255}Fm($7/2^+$), two and eight decaying modes with no change in parity precede the first appearing decay mode involving a change in parity to ^{247}Cm ($11/2^-$, 0.062 MeV, 12.5%, $\ell_{\rm min} = 5$) and ^{251}Cf ($9/2^-$, 0.434 MeV, 0.036%, $\ell_{\rm min} = 1$), respectively. The highest intense decaying modes of ^{251}Cf($1/2^+$) and ^{255}Fm($7/2^+$) are their

TABLE I. The ratios of the α-preformation factor for the unfavored decay modes displayed in Figs. 2–4 to that of the corresponding favored modes. The calculated S_α(unfavored)/S_α(favored) ratios for the unfavored decay modes between states of the same parity (column 4) are compared to that for the decay modes involving a change in parity (column 5). $J^\pi_{n=2,3,4,5}$ represent the higher excited states having the same spin-parity assignments J^π. The different states of the same nucleus are listed in an ascending order according to their energy.

Decay mode 1 (favored)	Decay mode 2 (unfavored, no change in parity)	Decay mode 3 (unfavored, a change in parity)	$S_\alpha(2)/S_\alpha(1)$	$S_\alpha(3)/S_\alpha(1)$
^{226}Th(0^+) → ^{222}Ra(0^+)$_{GS}$	^{226}Th(0^+) → ^{222}Ra(2^+)	^{226}Th(0^+) → ^{222}Ra(1^-)	1.3433	0.0255
	^{226}Th(0^+) → ^{222}Ra(4^+)	^{226}Th(0^+) → ^{222}Ra(3^-)	0.4243	0.2541
	^{226}Th(0^+) → ^{222}Ra(2^+_2)	^{226}Th(0^+) → ^{222}Ra((5^-))	0.5959	0.0097
^{228}Th(0^+) → ^{224}Ra(0^+)$_{GS}$	^{228}Th(0^+) → ^{224}Ra(2^+)	^{228}Th(0^+) → ^{224}Ra(1^-)	1.3196	0.1262
	^{228}Th(0^+) → ^{224}Ra(4^+)	^{228}Th(0^+) → ^{224}Ra((3^-))	0.6696	0.0875
	^{228}Th(0^+) → ^{224}Ra((6^+))	^{228}Th(0^+) → ^{224}Ra((5^-))	0.0179	0.0011
	^{228}Th(0^+) → ^{224}Ra((2^+_2))		0.3688	
^{230}Th(0^+) → ^{226}Ra(0^+)$_{GS}$	^{230}Th(0^+) → ^{226}Ra(2^+)	^{230}Th(0^+) → ^{226}Ra(1^-)	1.0224	0.0350
	^{230}Th(0^+) → ^{226}Ra(4^+)	^{230}Th(0^+) → ^{226}Ra(3^-)	0.4157	0.0105
	^{230}Th(0^+) → ^{226}Ra(6^+)	^{230}Th(0^+) → ^{226}Ra(5^-)	0.0103	0.0069
	^{230}Th(0^+) → ^{226}Ra(2^+_2)		0.5007	
^{225}Th($3/2^+$) → ^{221}Ra(($3/2^+$))$_{Ex}$	^{225}Th($3/2^+$) → ^{221}Ra($5/2^+$)$_{GS}$	^{225}Th($3/2^+$) → ^{221}Ra(($5/2^-$))	0.0179	0.0070
	^{225}Th($3/2^+$) → ^{221}Ra($7/2^+$)	^{225}Th($3/2^+$) → ^{221}Ra(($7/2^-$))	0.0227	0.0417
	^{225}Th($3/2^+$) → ^{221}Ra(($7/2^+_2$))	^{225}Th($3/2^+$) → ^{221}Ra($5/2^-_2$)	0.4675	0.2024
	^{225}Th($3/2^+$) → ^{221}Ra(($5/2^+_2$))	^{225}Th($3/2^+$) → ^{221}Ra($3/2^-, 5/2^-_3$)	0.9014	0.2891
^{251}Cf($1/2^+$) → ^{247}Cm($1/2^+$)$_{Ex}$	^{251}Cf($1/2^+$) → ^{247}Cm($5/2^+$)	^{251}Cf($1/2^+$) → ^{247}Cm($9/2^-$)$_{GS}$	0.1394	0.0078
	^{251}Cf($1/2^+$) → ^{247}Cm(($7/2^+$))	^{251}Cf($1/2^+$) → ^{247}Cm($11/2^-$)	0.1242	0.0784
	^{251}Cf($1/2^+$) → ^{247}Cm(($7/2^+_2$))	^{251}Cf($1/2^+$) → ^{247}Cm($13/2^-$)	0.0996	0.1056
	^{251}Cf($1/2^+$) → ^{247}Cm($9/2^+$)		0.2193	
	^{251}Cf($1/2^+$) → ^{247}Cm(($9/2^+_2$))		0.0698	
	^{251}Cf($1/2^+$) → ^{247}Cm($3/2^+$)		0.2399	
	^{251}Cf($1/2^+$) → ^{247}Cm(($5/2^+_2$))		0.4398	
	^{251}Cf($1/2^+$) → ^{247}Cm(($7/2^+_3$))		0.8524	
	^{251}Cf($1/2^+$) → ^{247}Cm(($3/2^+_2$))		0.2305	
	^{251}Cf($1/2^+$) → ^{247}Cm(($5/2^+_3$))		0.1483	
^{255}Fm($7/2^+$) → ^{251}Cf($7/2^+$)$_{Ex}$	^{255}Fm($7/2^+$) → ^{251}Cf($1/2^+$)$_{GS}$	^{255}Fm($7/2^+$) → ^{251}Cf($11/2^-$)	0.0017	0.0073
	^{255}Fm($7/2^+$) → ^{251}Cf($3/2^+$)	^{255}Fm($7/2^+$) → ^{251}Cf($9/2^-$)	0.0008	0.0126
	^{255}Fm($7/2^+$) → ^{251}Cf($5/2^+$)	^{255}Fm($7/2^+$) → ^{251}Cf(($3/2^-$))	0.0042	2×10^{-5}
	^{255}Fm($7/2^+$) → ^{251}Cf($9/2^+$)	^{255}Fm($7/2^+$) → ^{251}Cf(($7/2^-$))	0.0036	1×10^{-5}
	^{255}Fm($7/2^+$) → ^{251}Cf($9/2^+_2$)	^{255}Fm($7/2^+$) → ^{251}Cf(($1/2^-$))	0.1688	2×10^{-5}
	^{255}Fm($7/2^+$) → ^{251}Cf($3/2^+_2$)	^{255}Fm($7/2^+$) → ^{251}Cf(($5/2^-$))	0.0008	4×10^{-5}
	^{255}Fm($7/2^+$) → ^{251}Cf($5/2^+_2$)	^{255}Fm($7/2^+$) → ^{251}Cf(($5/2^-_2$))	0.0009	0.0036
	^{255}Fm($7/2^+$) → ^{251}Cf($11/2^+$)	^{255}Fm($7/2^+$) → ^{251}Cf(($3/2^-_2$))	0.0429	0.0166
	^{255}Fm($7/2^+$) → ^{251}Cf(($13/2^+$))	^{255}Fm($7/2^+$) → ^{251}Cf(($5/2^-_3$))	0.0036	0.0082
	^{255}Fm($7/2^+$) → ^{251}Cf($9/2^+_3$)	^{255}Fm($7/2^+$) → ^{251}Cf(($7/2^-_2$))	0.0003	0.0074
	^{255}Fm($7/2^+$) → ^{251}Cf(($11/2^+_2$))	^{255}Fm($7/2^+$) → ^{251}Cf(($9/2^-_2$))	0.0004	0.0056
	^{255}Fm($7/2^+$) → ^{251}Cf(($15/2^+$))	^{255}Fm($7/2^+$) → ^{251}Cf($9/2^-_3$)	0.0217	0.0039
	^{255}Fm($7/2^+$) → ^{251}Cf(($5/2^+_3$))	^{255}Fm($7/2^+$) → ^{251}Cf($11/2^-_2$)	0.0277	0.0136
	^{255}Fm($7/2^+$) → ^{251}Cf($9/2^+_4$)		0.0153	
	^{255}Fm($7/2^+$) → ^{251}Cf(($3/2^+_3$))		0.0008	
	^{255}Fm($7/2^+$) → ^{251}Cf(($9/2^+_5$))		0.0048	
^{235}U($7/2^-$) → ^{231}Th($7/2^-$)$_{Ex}$	^{235}U($7/2^-$) → ^{231}Th($5/2^-$)	^{235}U($7/2^-$) → ^{231}Th($5/2^+$)$_{GS}$	0.0209	0.0008
	^{235}U($7/2^-$) → ^{231}Th($9/2^-$)	^{235}U($7/2^-$) → ^{231}Th($7/2^+$)	0.3059	0.0013
	^{235}U($7/2^-$) → ^{231}Th(($11/2^-$))	^{235}U($7/2^-$) → ^{231}Th($9/2^+$)	0.1303	0.0012
	^{235}U($7/2^-$) → ^{231}Th(($13/2^-$))	^{235}U($7/2^-$) → ^{231}Th($11/2^+$)	0.0916	0.0019
	^{235}U($7/2^-$) → ^{231}Th($9/2^-_2$)	^{235}U($7/2^-$) → ^{231}Th($3/2^+$)	0.3220	0.0038
	^{235}U($7/2^-$) → ^{231}Th($11/2^-_2$)	^{235}U($7/2^-$) → ^{231}Th($5/2^+_2$)	0.0845	0.0030
		^{235}U($7/2^-$) → ^{231}Th($7/2^+_2$)		0.0050
		^{235}U($7/2^-$) → ^{231}Th($5/2^+_3$)		0.0003
		^{235}U($7/2^-$) → ^{231}Th($5/2^+_4$))		0.0057
		^{235}U($7/2^-$) → ^{231}Th(($9/2^+_2$))		0.0020
		^{235}U($7/2^-$) → ^{231}Th($7/2^+_3$)		0.0075
		^{235}U($7/2^-$) → ^{231}Th(($7/2^+_4$))		0.0150

TABLE I. (*Continued.*)

Decay mode 1 (favored)	Decay mode 2 (unfavored, no change in parity)	Decay mode 3 (unfavored, a change in parity)	$S_\alpha(2)/S_\alpha(1)$	$S_\alpha(3)/S_\alpha(1)$
		$^{235}\mathrm{U}(7/2^-) \rightarrow {}^{231}\mathrm{Th}((11/2^+_2))$		0.0091
$^{243}\mathrm{Am}(5/2^-) \rightarrow {}^{239}\mathrm{Np}(5/2^-)_{\mathrm{GS}}$	$^{243}\mathrm{Am}(5/2^-) \rightarrow {}^{239}\mathrm{Np}(7/2^-)$	$^{243}\mathrm{Am}(5/2^-) \rightarrow {}^{239}\mathrm{Np}(5/2^+)$	0.4414	0.0012
	$^{243}\mathrm{Am}(5/2^-) \rightarrow {}^{239}\mathrm{Np}(9/2^-)$	$^{243}\mathrm{Am}(5/2^-) \rightarrow {}^{239}\mathrm{Np}(7/2^+)$	0.1194	0.0014
	$^{243}\mathrm{Am}(5/2^-) \rightarrow {}^{239}\mathrm{Np}((11/2^-))$	$^{243}\mathrm{Am}(5/2^-) \rightarrow {}^{239}\mathrm{Np}((5/2^+_2))$	0.0074	0.0013
	$^{243}\mathrm{Am}(5/2^-) \rightarrow {}^{239}\mathrm{Np}((13/2^-))$	$^{243}\mathrm{Am}(5/2^-) \rightarrow {}^{239}\mathrm{Np}((7/2^+_2, 9/2^+))$	0.0090	0.0008
		$^{243}\mathrm{Am}(5/2^-) \rightarrow {}^{239}\mathrm{Np}((9/2^+))$		0.0026
		$^{243}\mathrm{Am}(5/2^-) \rightarrow {}^{239}\mathrm{Np}((11/2^+))$		0.0008
$^{247}\mathrm{Cm}(9/2^-) \rightarrow {}^{243}\mathrm{Pu}(9/2^-)_{\mathrm{Ex}}$	$^{247}\mathrm{Cm}(9/2^-) \rightarrow {}^{243}\mathrm{Pu}(11/2^-)$	$^{247}\mathrm{Cm}(9/2^-) \rightarrow {}^{243}\mathrm{Pu}(7/2^+)_{\mathrm{GS}}$	0.2827	0.0005
		$^{247}\mathrm{Cm}(9/2^-) \rightarrow {}^{243}\mathrm{Pu}(9/2^+)$		0.0005
		$^{247}\mathrm{Cm}(9/2^-) \rightarrow {}^{243}\mathrm{Pu}(11/2^+)$		0.0003
		$^{247}\mathrm{Cm}(9/2^-) \rightarrow {}^{243}\mathrm{Pu}(5/2^+)$		0.0142
		$^{247}\mathrm{Cm}(9/2^-) \rightarrow {}^{243}\mathrm{Pu}(7/2^+_2)$		0.0089

decays to the excited states $1/2^+$ (0.405 MeV, 35.4%, $\ell_{\min} = 0$) and $7/2^+$ (0.106 MeV, 93.4%, $\ell_{\min} = 0$) of ^{247}Cm and ^{251}Cf, respectively, with the same spin-parity assignments. The decays of $^{251}\mathrm{Cf}(1/2^+)$ and $^{255}\mathrm{Fm}(7/2^+)$ to the ground states of ^{247}Cm ($9/2^-$, 0 MeV, 2.6%, $\ell_{\min} = 5$) and ^{251}Cf ($1/2^+$, 0 MeV, 0.07%, $\ell_{\min} = 4$), respectively, take places as the eighth intense decay modes because of the large $\ell_{\min}$ in addition to the change in parity in the former decay. Figure 3(b) shows the intensity of 21 decay modes of $^{255}\mathrm{Fm}(7/2^+)$ with no change in parity (solid circles) and 13 modes with a parity change (open circles) to ^{251}Cf in its ground and different excited states, as a function of $\ell_{\min}$. As shown in Fig. 3(a), the different decay modes for which the parity remains unchanged yield higher maximum and minimum preformation factor $S_\alpha(\ell_{\min})$ than those extracted for the decay modes with a parity change. The S_α(unfavored)/S_α(favored) ratios for the unfavored decay modes of the $^{225}\mathrm{Th}(3/2^+)$, $^{251}\mathrm{Cf}(1/2^+)$, and $^{255}\mathrm{Fm}(7/2^+)$ nuclei relative to their corresponding favored decays are added to Table I. This ratio for the unfavored decay modes of ^{225}Th and ^{251}Cf, between states of similar parities, is obtained within the ranges from 0.018 to 0.901 (with an average value of 0.352) and from 0.070 to 0.852 (with an average value of 0.256), respectively. The similar unfavored decay modes of ^{255}Fm yield S_α(unfavored)/S_α(favored) ratios ranging between 0.0003 and 0.1688 (with an average value of 0.0186). The same ratios for the unfavored decay modes of the three mentioned nuclei but between states of different parities show less values down to 10^{-5}, with average values of 0.135, 0.064, and 0.006, respectively. Moreover, while the local maxima of the oscillatory trend of $S_\alpha^{\mathrm{ave}}(\ell_{\min})$ in Fig. 3(a) are obtained at the even $\ell_{\min}$, values where there is no change in parity, the coexisting local minima are obtained for the odd $\ell_{\min}$ values that recognize a parity change. This trend estimate an absent local maxima of S_α^{ave} at $\ell_{\min} = 6$ for which there is no observed decay mode for the presented nuclei. The extracted preformation factors and the intensities of the different α-decay modes displayed in Fig. 3 underline the hindrance in decay modes that require a change in parity.

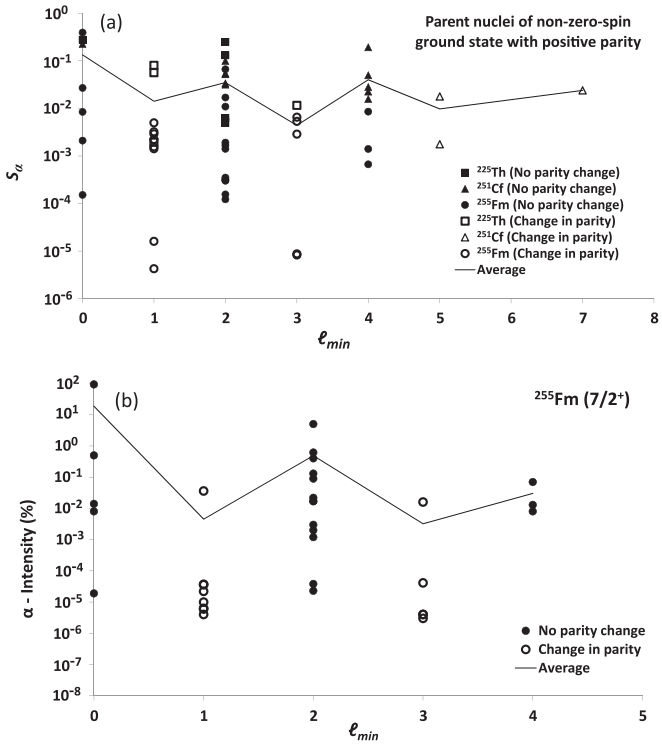

FIG. 3. (a) Same as Fig. 2(a), but for the even-odd nuclei of $^{225}\mathrm{Th}(3/2^+)$, $^{251}\mathrm{Cf}(1/2^+)$, and $^{255}\mathrm{Fm}(7/2^+)$. (b) Same as Fig. 2(c), but for the $^{255}\mathrm{Fm}(7/2^+)$ isotope.

Figure 4(a) shows the estimated preformation factor for the different decay modes of the $^{235}\mathrm{U}(7/2^-)$, $^{243}\mathrm{Am}(5/2^-)$, and $^{247}\mathrm{Cm}(9/2^-)$ parent nuclei in their ground states into the ground and excited states of their ^{231}Th, ^{239}Np, and ^{243}Pu daughter nuclei. These parent nuclei in their non-zero-spin with negative parity ground states principally decay via α emission with intensity of about 100%, in addition to a very little contribution of spontaneous fission (^{235}U, ^{243}Am) and cluster decay modes (^{235}U) of tiny branching ratios less than 10^{-9}%. The α-decay modes taking places between states of different parities represent only about 12%, 0.4% and 24% of the full α-decay intensity of $^{235}\mathrm{U}(7/2^-)$, $^{243}\mathrm{Am}(5/2^-)$, and $^{247}\mathrm{Cm}(9/2^-)$, respectively. Regarding $^{235}\mathrm{U}(7/2^-)$, the most intense decay modes were marked to the three excited

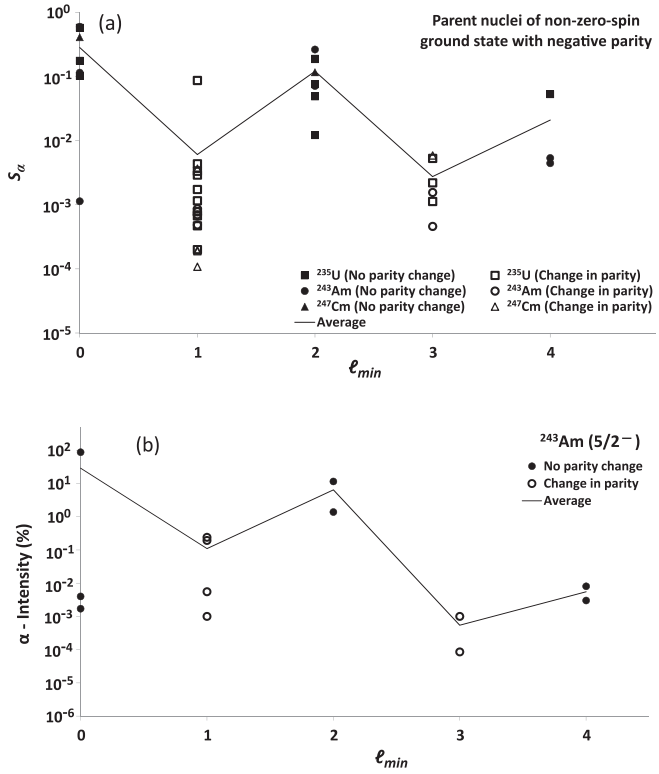

FIG. 4. (a) Same as Fig. 2(a), but for the even-odd nuclei of ^{235}U(7/2$^-$), ^{243}Am(5/2$^-$), and ^{247}Cm(9/2$^-$). (b) Same as Fig. 2(c), but for the ^{243}Am(5/2$^-$) isotope.

states 7/2$^-$ ($E = 0.205$ MeV, $I_\alpha = 57.73\%$, $\ell_{\min} = 0$), 9/2$^-$ (0.237 MeV, 18.92%, 2), and 7/2$^-$ (0.388 MeV, 6.01%, 0) of ^{231}Th. These three states have the same parity of ^{235}U(7/2$^-$). The decay to the ground state of ^{231}Th (5/2$^+$ (0 MeV, 4.77%, 1)), which has a different parity than that of ^{235}U(7/2$^-$), was reported as the fourth intense decay mode. On the other hand, the decay mode to ^{243}Pu in its excited state 9/2$^-$ (0.403 MeV, 71%, $\ell_{\min} = 0$) that has the same spin-parity assignment of the parent nucleus ^{247}Cm(9/2$^-$) precede five decay modes to lower-lying states of ^{243}Pu of different parity assignment, including the decay to the ground state of ^{243}Pu (7/2$^+$, 0 MeV, 13.8%, $\ell_{\min} = 1$). For ^{243}Am (5/2$^-$), three intense decay modes with no parity change exceed the highest observed intensity of a decay mode demanding a change in parity, to the ground state of ^{239}Np (5/2$^+$, 0 MeV, 0.24%, $\ell_{\min} = 1$). Shown in Fig. 4(b) is the intensity of seven decay modes of ^{243}Am(5/2$^-$) to excited states of ^{239}Np having the same parity and six decay modes involving a change in parity, as a function of $\ell_{\min}$. While the sum of the intensities of the decays between states of the same parity is about 99.56%, the sum corresponding to decays with a change in parity involved is about 0.44%. As presented in Table I, the S_α(unfavored)/S_α(favored) ratios for the unfavored decays of ^{235}U(7/2$^-$), ^{243}Am(5/2$^-$), and ^{247}Cm(9/2$^-$) in which the parity remains unchanged show average values of 0.159, 0.144, and 0.283, respectively. The corresponding unfavored decay modes involving a change in parity yield less average values of the S_α (unfavored)/S_α(favored) ratio of about 0.004, 0.001, and 0.005, respectively. Figures 4(a) and 4(b), and Table I, reinforce that the decay modes between states of different parity yield smaller preformation factor and exhibit less intensity, relative to the decays involving states of the same parity.

IV. SUMMARY AND CONCLUSION

We investigated the unfavored α-decay modes between states of different parities. The decays from the GS of parent nuclei to the ground and different excited states of daughter nuclei were considered. Aside from the reported enhancement of the favored decays, we found that the nuclei that unfavorably decay to daughters of different ground-state parity exhibit relatively larger half-life and less α-decay intensity than the nuclei that unfavorably decay to daughters of different GS spin but with the same parity. Likewise, the α-decay modes of a given nucleus to states of its daughter with a different parity show larger partial half-life relative to the corresponding unfavored decays between states of the same parity. In particular, the total α intensity of a given nucleus mostly appears via its decay modes to states of the same spin-parity configurations, then through decay modes to states of different spin but with the same parity. The decay modes between states of different parities come in the third order with the smallest fraction of intensity. In a similar vein, we found that for a parent nucleus with a specific spin-parity configuration, the preformation factor of an α cluster leaving a daughter with a different parity is less than if the daughter nucleus has the same parity of parent but with a different spin. Accordingly, the interesting conclusion that can be drawn from our investigation is that the change in parity between the state of the α emitter and that of its daughter nucleus hinders the α-decay mode between these states and increases (decreases) the corresponding partial half-life (decay intensity). This hindrance exceeds that of the unfavored decays between states of the same parity, and abolishes the enhancement from the expected increase in the Q_α value of the odd-A isotopes relative to the even-even ones.

[1] S. Hofmann and G. Munzenberg, Rev. Mod. Phys. **72**, 733 (2000).
[2] Yu. Ts. Oganessian *et al.*, Phys. Rev. Lett. **104**, 142502 (2010).
[3] Yu. Ts. Oganessian and K. P. Rykaczewski, Phys. Today **68**(8), 32 (2015).
[4] W. M. Seif, Phys. Rev. C **91**, 014322 (2015).
[5] D. Bai and Z. Ren, Phys. Lett. B **786**, 5 (2018).
[6] K. P. Santhosh and C. Nithya, Atm. Data Nucl. Data Tables **119**, 33 (2018).
[7] M. Ismail and A. Adel, Phys. Rev. C **97**, 044301 (2018).
[8] D. S. Delion, Z. Ren, A. Dumitrescu, and D. Ni, J. Phys. G: Nucl. Part. Phys. **45**, 053001 (2018).
[9] M. Ismail, W. M. Seif, A. Adel, and A. Abdurrahman, Nucl. Phys. A **958**, 202 (2017).

[10] M. Ismail, A. Y. Ellithi, M. M. Botros, and A. Adel, Phys. Rev. C **81**, 024602 (2010).
[11] D. Ni, Z. Ren, T. Dong, and Y. Qian, Phys. Rev. C **87**, 024310 (2013).
[12] W. M. Seif, N. V. Antonenko, G. G. Adamian, and Hisham Anwer, Phys. Rev. C **96**, 054328 (2017).
[13] Y. Qian and Z. Ren, J. Phys. G: Nucl. Part. Phys. **45**, 085103 (2018).
[14] W. M. Seif and A. Abdurrahman, Chin. Phys. C **42**, 014106 (2018).
[15] D. Ni and Z. Ren, Phys. Rev. C **92**, 054322 (2015).
[16] M. Ismail and A. Adel, Phys. Rev. C **89**, 034617 (2014).
[17] W. M. Seif, Phys. Rev. C **74**, 034302 (2006).
[18] E. Shin, Y. Lim, C. Ho Hyun, and Y. Oh, Phys. Rev. C **94**, 024320 (2016).
[19] W. M. Seif, M. Shalaby, and M. F. Alrakshy, Phys. Rev. C **84**, 064608 (2011).
[20] M. Ismail, A. Adel, and M. M. Botros, Phys. Rev. C **93**, 054618 (2016).
[21] M. Ismail and A. Adel, Phys. Rev. C **90**, 064624 (2014).
[22] M. Ismail and A. Adel, Phys. Rev. C **88**, 054604 (2013).
[23] M. Ismail and A. Adel, Phys. Rev. C **86**, 014616 (2012).
[24] J. Dong, W. Zuo, and J. Gu, Phys. Rev. C **87**, 014303 (2013).
[25] W. M. Seif and A. S. Hashem, Chin. Phys. C **42**, 064104 (2018).
[26] Y. L. Zhang and Y. Z. Wang, Phys. Rev. C **97**, 014318 (2018).
[27] W. M. Seif and L. H. Amer, Nucl. Phys. A **969**, 254 (2018).
[28] H. Badran *et al.*, Phys. Rev. C **96**, 064314 (2017).
[29] D. Ni and Z. Ren, Phys. Rev. C **83**, 067302 (2011).
[30] D. Ni and Z. Ren, Phys. Rev. C **86**, 054608 (2012).
[31] K. P. Santhosh, J. G. Joseph, and B. Priyanka, Nucl. Phys. A **877**, 1 (2012).
[32] K. P. Santhosh and J. G. Joseph, Phys. Rev. C **86**, 024613 (2012).
[33] A. Adel and T. Alharbi, Phys. Rev. C **92**, 014619 (2015).
[34] D. S. Delion, Monika Patial, R. J. Liotta, and R. Wyss, J. Phys. G: Nucl. Part. Phys. **43**, 095109 (2016).
[35] D. S. Delion, A. Dumitrescu, and V. V. Baran, Phys. Rev. C **93**, 044321 (2016).
[36] M. Mirea, Phys. Rev. C **96**, 064607 (2017).
[37] M. Mirea, Europhys Lett. **124**, 12001 (2018).
[38] A. Adel and T. Alharbi, Nucl. Phys. A **975**, 1 (2018).
[39] J. Dong, H. Zhang, Y. Wang, W. Zuo, and J. Li, Nucl. Phys. A **832**, 198 (2010).
[40] D. Ni and Z. Ren, Phys. Rev. C **81**, 064318 (2010).
[41] K. P. Santhosh, S. Sahadevan, and J. G. Joseph, Nucl. Phys. A **850**, 34 (2011).
[42] A. N. Andreyev *et al.*, Phys. Rev. Lett. **82**, 1819 (1999).
[43] S. A. Karamian, J. J. Carroll, S. Iliev, and S. P. Tretyakova, Phys. Rev. C **75**, 057301 (2007).
[44] S. M. S. Ahmed, R. Yahaya, S. Radiman, and M. S. Yasir, J. Phys. G: Nucl. Part. Phys. **40**, 065105 (2013).
[45] D. Deng, Z. Ren, D. Ni, and Y. Qian, J. Phys. G: Nucl. Part. Phys. **42**, 075106 (2015).
[46] D. Deng and Z. Ren, Phys. Rev. C **93**, 044326 (2016).
[47] S. M. S. Ahmed, Nucl. Phys. A **962**, 103 (2017).
[48] W. M. Seif, J. Phys. G: Nucl. Part. Phys. **40**, 105102 (2013).
[49] C. Xu, G. Röpke, P. Schuck, Z. Ren, Y. Funaki, H. Horiuchi, A. Tohsaki, T. Yamada, and B. Zhou, Phys. Rev. C **95**, 061306(R) (2017).
[50] Y. Qian and Z. Ren, J. Phys. G: Nucl. Part. Phys. **45**, 035103 (2018).
[51] Y. Qian and Z. Ren, Scie. China Phys. Mech. Astron. **56**, 1520 (2013).
[52] H. Koura and S. Chiba, Phys. Rev. C **95**, 064304 (2017).
[53] Computer code NUDAT2.7, Nuclear Structure and Decay Data, http://www.nndc.bnl.gov/nudat2/.
[54] N. G. Kelkar and H. M. Castaneda, Phys. Rev. C **76**, 064605 (2007).
[55] N. Anantaraman, H. Toki, and G. F. Bertsch, Nucl. Phys. A **398**, 269 (1983).
[56] E. Chabanat, P. Bonche, P. Haensel *et al.*, Nucl. Phys. A **635**, 231 (1998).
[57] C. Xu and Z. Ren, Nucl. Phys. A **753**, 174 (2005).
[58] R. E. Langer, Phys. Rev. **51**, 669 (1937).
[59] G. R. Satchler and W. G. Love, Phys. Rep. **55**, 183 (1979).
[60] Dao T. Khoa, Phys. Rev. C **63**, 034007 (2001).
[61] V. Yu. Denisov and W. Nörenberg, Eur. Phys. J. A **15**, 375 (2002).
[62] Raj K. Gupta, D. Singh, and W. Greiner, Phys. Rev. C **75**, 024603 (2007).
[63] D. Vautherin and D. M. Brink, Phys. Rev. C **5**, 626 (1972).
[64] G. Audi, F. G. Kondev, Meng Wang, W. J. Huang, and S. Naimi, Chin. Phys. C **41**, 030001 (2017).
[65] M. Wang, G. Audi, F. G. Kondev, W. J. Huang, S. Naimi, and Xing Xu, Chin. Phys. C **41**, 030003 (2017).
[66] M. S. Basunia, Nucl. Data Sheets **107**, 2323 (2006).